



INVERSE-DESIGNED NANOPHOTONIC RESONATORS FOR
CAVITY QUANTUM ELECTRODYNAMICS WITH DIAMOND
COLOR CENTERS

Jean-Michel Borit

Stanford University

May 2024

An honors thesis submitted to the department of
Physics
in partial fulfillment of the requirements for the undergraduate
honors program

Advisor: Jelena Vučković

_____ Date: _____

Jelena Vučković (Thesis Advisor)

Jensen Huang Professor in Global Leadership

Electrical Engineering and, by courtesy, Applied Physics

_____ Date: _____

Jason Hogan (Thesis Advisor)

Associate Professor

Physics

To my grandmother, Julia Salinas, with love and gratitude

Abstract

In recent years, inverse design has emerged as a powerful method for applications in nanophotonics, yielding non-intuitive device geometries that exhibit a comparable performance to their traditional counterparts. In this thesis, we provide optimal inverse designs of nanophotonic resonators for cavity quantum electrodynamics with diamond color centers. Color centers, optically active spin defects in diamond, hold vast promise for applications in quantum networks. However, their potential is hindered by low photon collection rates in bulk. In this work, we employ the latest developments in inverse design capabilities to optimize diamond Fabry-Pérot microcavities. These microcavities enhance color center emission in the zero-phonon line via the Purcell effect, allowing for significantly higher collection rates. As a material, diamond has long remained challenging for inverse design, owing to constraints in processing and fabrication. The recent advent of diamond thin-films now allows for the full potential of inverse design, and could pave the way for scalable, diamond-based quantum networks.

Acknowledgements

First and foremost, I would like to express my gratitude to my thesis advisor, Prof. Jelena Vučković, for her continued support and mentorship during my three years at the Nanoscale and Quantum Photonics Lab. Jelena provided all the equipment, laboratory space, facilities, and resources needed for this project. Since my freshman year, Jelena has nurtured my scientific curiosity, as well as my passion for quantum information science and photonics. Her academic and professional guidance have been hugely helpful throughout my time at Stanford.

Scientific research is a transformative and life-changing experience. While it provides a huge sense of personal fulfillment, intellectual vitality, and happiness, it also comes with its own frustrations and difficulties. Having dedicated, caring mentors is a critical ingredient to overcoming these challenges. I would like to thank Hope Lee and Jakob Grzesik for having fulfilled this role. Hope and Jakob are truly wonderful to work with, and I am looking forward to continuing my research alongside them next academic year, as part of my M.S. candidacy.

The work presented in this thesis would not have been possible without the help of Dr. Jesse Lu, from SPINS Photonics. Jesse developed a significant portion of the computational software employed in this research. His constant support was critical during the early stages of this project. Jesse's insights on inverse design and *fdtd-z* helped build the foundations upon which this research project was established.

I would like to express my gratitude to Dr. Daniel Riedel for introducing me to the field of photonics. Daniel was my first mentor at the lab. His mentorship was key during my freshman and sophomore years. To a significant extent, by ability to pursue this research project is a result of his support and guidance during my

early years in the group. I would also like to thank Prof. Chris Anderson for serving the role of an unofficial mentor during his brief time at Stanford. Chris' vision and creativity were inspirational. He was always eager to provide advice and help others.

Similarly, I would like to thank all members of the Vučković group who have I have had the pleasure to work with throughout my undergraduate career: Dominic Catanzaro, Abby Stein, Hannah Kleidermacher, Alison Rugar, Daniil Lukin, Jinhie Skarda, Melissa Guidry, Eric Rosenthal, Alex White, Joshua Yang, and Geun Ho Ahn. I also would like to thank Prof. David Miller and Prof. Joonhee Choi for fruitful discussions.

Finally, I would like to express my most heartfelt sense of gratitude to my family and friends. My parents, my sister, and grandparents are one of the biggest joys in my life. I have no words to express how thankful I am for their unconditional love and support. My friends, whether they be in a different continent or a bike ride away, have also been incredibly supportive of my passion for science, and have helped both my personal and intellectual growth since my arrival to Stanford.

Contents

1	Introduction	3
2	Theoretical Background	5
2.1	Towards the Quantum Internet	5
2.1.1	Quantum Networks	5
2.1.2	Color Centers in Diamond: an Ideal Quantum Memory	8
2.1.3	Group-IV Color Centers and the Tin-Vacancy Center	9
2.2	Cavity QED	12
2.2.1	Nanophotonic Resonators	12
2.2.2	Cavity QED: the Strong and Weak Coupling Regimes	13
2.2.3	The Purcell Effect	15
2.2.4	The Quality Factor	16
2.3	Fabry-Pérot Resonators	17
2.3.1	The Resonance Condition in Fabry-Pérot Resonators	17
2.3.2	Calculating Q -Factors in Fabry-Pérot Resonators	18
2.4	Electromagnetic Simulation and Inverse Design	19
2.4.1	The Finite-Difference Time-Domain Method	20
2.4.2	Inverse Design	20
2.4.3	Made in Spilker: Prior Work on Inverse-Designed Mirrors	22
2.5	Chapter Summary	23
3	Mirror Design and Optimization	25
3.1	Inverse-Design Problem Formulation	25

3.1.1	The Scattering Matrix	26
3.1.2	Constraining Waveguide Dimensions	27
3.2	Inverse-Designed Reflectors	28
3.2.1	Optimization Recipe	28
3.2.2	Testing Mirror Performance	29
3.3	Chapter Summary	31
4	An Inverse-Designed Fabry-Pérot Resonator	32
4.1	Simulating High- Q Resonators	32
4.1.1	Optimizing Emitter Location	33
4.1.2	Simulation Setup	33
4.2	Resonator Optimization	34
4.2.1	Spacer Sweeping	34
4.2.2	Purcell Enhancement of Resulting Devices	36
4.3	Chapter Summary	37
5	Summary and Outlook	38
	Bibliography	40

List of Tables

2.1 Energy splitting and ZPLs in different group-IV centers 11

List of Figures

2.1	Group-IV color centers in the periodic table	8
2.2	Energy diagram of a group-IV color center at zero magnetic field . . .	9
2.3	Ground-state manifold of a generic group-IV color center under a mag- netic field	10
2.4	A generic two-level system	13
2.5	An inverse-designed reflector	22
3.1	Physical setup for a generic scattering matrix	26
3.2	An electric field inside a diamond waveguide	27
3.3	Inverse-design optimization of a single mirror	29
3.4	Transmission simulation set-up	30
3.5	Simulated reflector performance	31
4.1	Q -factor simulation setup	34
4.2	Q -factors of resulting devices	35
4.3	Inverse-designed resonator spectrum for $L = 5 \mu\text{m}$	35
4.4	Resonant modes in our FP resonators	35
4.5	Purcell enhancement of resulting devices	36

Chapter 1

Introduction

Quantum information processing focuses on the manipulation of quantum bits of information (qubits) [1, 2]. Unlike classical bits, which exist as well-defined, binary states, qubits are more accurately characterized by a continuum of possible states. Instead of being described by two discrete values, a 0 or a 1, qubits can take any linear combination of $|0\rangle$ and $|1\rangle$ basis vectors [3]. This feature, formally known as quantum superposition, allows for several fascinating applications, and has propelled the field of quantum science and technology (QST) with tremendous momentum over the past decades [4, 5].

High-fidelity quantum protocols hold vast promise for applications in sensing and metrology [6, 7]. Furthermore, through quantum computing, the field of quantum information science promises to solve previously intractable problems in computer science and optimization [8, 9]. In recent years, the field of quantum engineering has seen incredible advancements [10, 11]. Thanks to breakthroughs in laser technology, AMO physics, temperature control, and material science, we now have the ability to prepare atoms, spin systems and photons in well-defined quantum states [11]. We are able to reliably manipulate these states –and to measure their time-evolution with unprecedented precision [11]. These developments pinpoint on the vast potential of quantum technologies, and have ignited a wave of research into scalable quantum systems across both industry and academia [12, 13].

Quantum communication is one of the most mature branches of QST [5]. Broadly

speaking, quantum communication refers to the body of research that seeks to efficiently transmit quantum information [5, 14]. Given two distinct quantum processing units, quantum communication researchers attempt to interconnect these, and have them exchange information without compromising the quality of their quantum states [14]. A paramount goal of quantum communication is the realization of scalable quantum networks, platforms that remotely connect quantum processors over distances spanning up thousands of kilometers [15]. As it will be explained later in this thesis, quantum networks could allow for fundamentally secure communication, ultra-fast quantum computation, distributed quantum simulation, and even quantum sensing [1, 2, 16].

Color centers, optically active impurities in diamond, have emerged as promising quantum network candidates based on their ability to support long-lived spin qubits and potential for integration with photonics for efficient spin control, initialization, and readout, as well as distribution of entanglement [17, 18]. At the Nanoscale and Quantum Photonics Lab, we seek to couple these emitters to photonic nanostructures in order to better control their optical emissions. The hope is to devise a highly coherent light-matter interface for scalable quantum network architectures. In this thesis, we explore inverse design as an avenue to optimize these nanostructures.

Inverse design is an automated photonics optimization framework [19, 20]. Over the past decade, it has emerged as a highly versatile resource for photonic nanotechnologies, owing to its high scalability and high-quality device yields [20, 21]. Here, we propose and study inverse-designed nanophotonic Fabry-Pérot resonators for cavity quantum electrodynamics with the tin-vacancy center in diamond. We outline the design, numerical simulation and quantum-mechanical features of these devices, setting the stage for their eventual fabrication and experimental characterization.

Chapter 2

Theoretical Background

2.1 Towards the Quantum Internet

As mentioned in the introduction, the overarching goal of this thesis is to design nanophotonic resonators that enhance the performance of color centers in quantum networks. In this section, we develop the fundamentals of color centers and quantum networks. We begin by motivating the development of quantum networks, and detail their basic requirements. We propose color centers as a physical platform for quantum networks. We introduce the tin-vacancy (SnV^-) center and outline its outstanding properties. Based on these properties, we choose this emitter as the focus of our thesis, thereby determining the target frequency at which we will subsequently optimize devices.

2.1.1 Quantum Networks

Quantum computers could offer faster, more powerful computation than their classical counterparts [22, 23]. They could also be employed to solve previously intractable problems in computer science [24]. By harnessing the intrinsic properties of quantum mechanics, quantum computers could allow for groundbreaking advances in physics, economics, finance, information processing, and biochemistry [25]. Just as the advent

of the internet allowed for non-local computing and long-distance information transmission, a so-called quantum network would permit distributed quantum computing and sensing, more efficient quantum simulation, and quantum key distribution¹ [26]. In order to understand the quantum internet, it is useful to review the basic concepts underlying everyday telecommunication schemes [27].

Telecommunication is based on the transmission of electromagnetic waves over large distances [28]. In practice, photons are the preferred mechanism for virtually all telecommunication schemes [28]. This is due to their low interaction rates with the environment and unparalleled high-speed transmission [28]. In order to efficiently transmit photons over large distances, it is relevant to consider losses over the chosen communication channel. Most commercial telecommunication optical fibers have losses nearing 0.2 dB/km [27]. This incredibly low loss translates to a transmission of 95% for a kilometer-long fiber, and repeaters can be used to amplify signals as they are transferred from their initial to their final location [27]. These repeaters ensure efficient, long-distance information transmission, and constitute the foundation of modern-day telecommunications [27].

Just as with classical information processing units, remotely connecting two quantum processors requires one to deal with signal attenuation [29]. For quantum systems, however, the no-cloning theorem applies [30]. This means that classical amplifiers cannot reproduce copies of a qubit [27]. Thus, for scalable quantum communication, rather than classical amplifiers, we require a quantum network, comprised of quantum repeaters that do not perturb the quality of transmitted quantum states [31].

Quantum repeaters are based on one of the most non-intuitive ideas underlying quantum mechanics: entanglement. Entanglement is one of the most foundational concepts of quantum information processing. It is a phenomenon where the quantum states of particles become instantaneously correlated regardless of distance. An interesting property of entanglement is that it can be swapped amongst different sets of entangled quantum systems. Consider the entangled states $|\Psi\rangle = \sum_n c_n |\psi_n^A\rangle \otimes |\psi_n^B\rangle$ and

¹Fundamentally secure encryption protocols that deterministically guarantee the detection of eavesdroppers during the establishment of a key

$|\Phi\rangle = \sum_n c_n |\psi_n^C\rangle \otimes |\psi_n^D\rangle$, where $|\psi_n^M\rangle$ represents the n -th basis vector of a system $|\psi_M\rangle$. In this case, entangling $|\psi_B\rangle$ and $|\psi_C\rangle$ (i.e., producing a state $|\Psi'\rangle = \sum_n c_n |\psi_n^B\rangle \otimes |\psi_n^C\rangle$) allows one to entangle systems $|\psi_A\rangle$ and $|\psi_D\rangle$ [27]. Under the quantum repeater approach, entanglement over any arbitrary distance L is possible by successively swapping entanglement between pairs through small sub-partitions of L over which photon loss is negligible [29]. In a scalable quantum network, multiple quantum repeaters (or “nodes”) are arranged in sequence to reliably transmit qubits across several kilometers.

Just as with classical telecommunications, photons are the preferred mechanism for quantum network architectures due to their low environment interaction rates and ultra-fast velocities. Beyond these two critical benefits, photonic quantum networks could also allow for easy-to-implement heralding schemes [32]. Under an efficient heralding scheme, one is able to determine whether or not entanglement was successfully achieved [27]. Consider, for instance, a pair of atoms, which we seek to entangle. It possible to generate entanglement between these two atoms through the detection of a photon that could have been emitted by either atom in the pair. In this case, the detection of a photon can help determine whether entanglement was established. If no photons are detected, the entanglement generation protocol can be re-initiated until it succeeds, thereby ensuring a successful swapping step in the quantum repeater link [27].

Photonic quantum networks have two critical requirements: (i) controllable stationary qubits with long coherences and (ii) efficient optical channels. Over the past decade, multiple physical platforms have been proposed as candidate quantum nodes [1, 15, 16]. Numerous quantum computing efforts across industry, including those led by Google and IBM, have been based on superconducting qubits [16]. While these qubits have remarkable properties, they require microwave frequencies and must be cooled to cryogenic temperatures to prevent Ohmic losses and overcome noisy channels [16]. Similarly, trapped ions, which stand out based on their homogeneity, require large optical set-ups, which makes scalability an outstanding challenge [16].

The figure shows a standard periodic table of elements. The elements in Group IV (Carbon, Silicon, Germanium, Tin, Lead, and Flerovium) are highlighted in yellow. The table includes element symbols, atomic numbers, and names. The lanthanide and actinide series are shown at the bottom.

Figure 2.1: Group-IV color centers in the periodic table

2.1.2 Color Centers in Diamond: an Ideal Quantum Memory

Color centers have emerged as very promising qubits due to their excellent optical coherences, short quantum gate times, and their ability to act as superb optical interfaces [17, 33, 34]. These defects allow for bound states within the bandgap by breaking translational symmetry on the diamond lattice structure [16]. Because such bound states resemble atomic energy levels and are optically-addressable, it is possible to employ them as controllable quantum bits [16]. In addition to their spin-dependent optical transitions and long-lived spin ground states, color centers hold vast potential for integration with nanophotonics due to their ability to act as single photon sources [17, 33]. This makes them an exquisite platform for scalable quantum network architectures. Because of these excellent features, multiple research groups in both academia and industry have dedicated significant resources to the study of color centers [18, 35]. Color centers have been at the heart of numerous state-of-the-art quantum network efforts, including QuTech’s three-node quantum network [36] and Amazon’s AWS quantum networking initiatives [37].

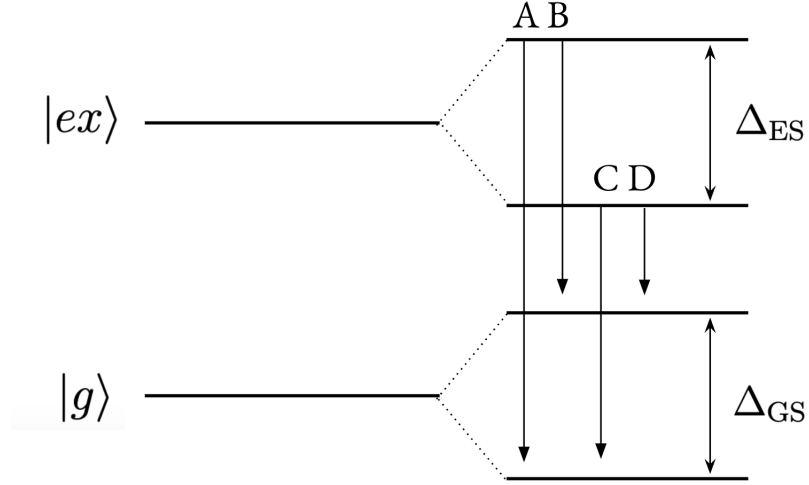


Figure 2.2: Energy diagram of a group-IV color center at zero magnetic field

2.1.3 Group-IV Color Centers and the Tin-Vacancy Center

Group-IV color centers, which will be our main focus of study in this thesis, are comprised of an interstitial group-IV impurity and two missing carbon atoms [16]. These color centers are characterized by inversion symmetry, a high-symmetry crystallographic axis along $\langle 111 \rangle$, and strong emission into their zero-phonon lines (ZPLs) [16]. Generally speaking, the emission of a color centers has two main components: the aforementioned ZPL and the phonon sideband (PSB) [16]. Photons in the ZPL are the result of relaxation from an excited state to the ground state via the emission of a single photon and no phonons [16]. This is the component of the spectrum that can be employed in quantum optics experiments requiring indistinguishable photons, such as entanglement generation [16]. Group-IV color centers have four zero-phonon lines (A, B, C and D) [16], as shown in Fig. 2.2. Relaxation via the emission of phonons and a photon, on the other hand, corresponds to the PSB [16].

Inversion symmetry implies that these defects lack a permanent dipole moment,

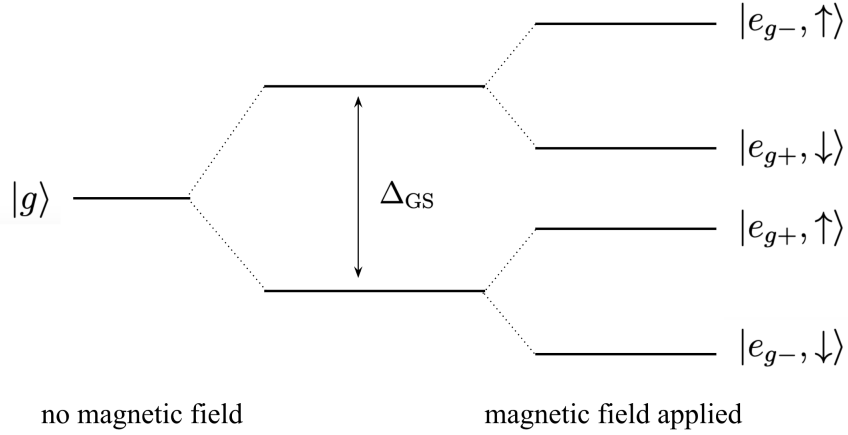


Figure 2.3: Ground-state manifold of a generic group-IV color center under a magnetic field

which makes them first-order insensitive to electric field fluctuations [16]. Furthermore, group-IV color centers have remarkably long coherences –on the order of hundreds of microseconds. Some of them, such as the tin-vacancy center, allow for operation at 1.7 K [16, 35], which is anticipated to have major implications for scalability and quantum architecture robustness.

Typically, using group-IV emitters as spin qubits requires lifting the two-fold spin degeneracy in the ground state [16]. This can be achieved through the application of a magnetic field (see Fig. 2.3). As discussed by Rugar in Ref. [16], by the Zeeman effect, in the presence of a magnetic field, the lower branch splits into $|e_{g-}, \downarrow\rangle$ and $|e_{g+}, \uparrow\rangle$. Similarly, the upper branch splits into $|e_{g+}, \downarrow\rangle$ and $|e_{g-}, \uparrow\rangle$. In this notation, the subscript of g denotes the even parity of the ground-state wave function. Similarly, the \pm in the subscript denotes an angular momentum number of $m_l = \pm 1$. In most applications, the lower branch, consisting of the pair $|e_{g-}, \downarrow\rangle$ and $|e_{g+}, \uparrow\rangle$, is employed as the qubit [16]. It is worthwhile noting that the degree of splitting in the ground and excited state manifolds is different for each species of color center. These differences in splitting are summarized in Table 2.1, which was adapted from Ref. [16].

The first negatively charged group-IV color center to be extensively studied was

Color center	Δ_{GS} (GHz)	ZPL (nm)
SiV ⁻	50	737
GeV ⁻	152	602
SnV ⁻	850	620

Table 2.1: Energy splitting and ZPLs in different group-IV centers

the SiV⁻ impurity [16]. This defect has been a protagonist in multiple quantum information processing demonstrations, including integrated quantum nodes, memory-enhanced quantum communication [38], and integration with nonlinear materials [39]. However, because of its 50 GHz ground state splitting, its operation is costly and hard-to-scale. Millisecond-long coherences can only be achieved at 100 mK [16]. This imposes several practical constraints and burdensome infrastructure requirements, such as dilution refrigerators and costly cryostats [16]. While this limitation can be mitigated, it requires specialized strain engineering on the sample [40].

Tin-vacancy centers, by contrast, have a significantly reduced phonon absorption rate at 1.7 K. At this temperature, tin-vacancies are expected to have a phonon absorption rate equal to that of silicon vacancies at 155 mK. SnV⁻ color centers also have a remarkable quantum efficiency (of as much as 80% at 1K) [16, 41]. Based on these favorable properties, tin-vacancies have gained considerable popularity in recent years, and are becoming an increasingly mature quantum emitter candidate. In 2021, a team in the Vučković group realized the first nanophotonic platform for these color centers [17]. This achievement marked a critical milestone in the study of SnV⁻ defects, and set the stage for a myriad of quantum engineering demonstrations, including microwave-based quantum control in 2023 [33, 42]. Driven by this momentum around SnV⁻ centers, we choose to optimize resonators for tin-vacancy emitters. As we will see in later chapters, this choice to use tin-vacancies will constrain our device space to cavities with resonances equal to the tin-vacancy ZPL. The effective, average wavelength of all four ZPL transitions in tin-vacancies is 620 nm [16]. Because of this reason, in this thesis, we will optimize devices using a target wavelength of 620 nm.

2.2 Cavity QED

Despite their exquisite properties and vast potential for applications in quantum information processing, color centers suffer from one important limitation: they have highly limited photon collection rates in bulk [17]. For this family of emitters, the ZPL spontaneous emission probability is limited, ranging from 3% (nitrogen-vacancies) to 30% (tin-vacancies) [43]. State-of-the-art quantum network efforts based on color center emitters, such as TU Delft’s three-node network, are severely limited by insufficient spontaneous emission, which severely hinders entanglement rates and precludes the realization of large-scale, multiparticle quantum communication. [36]. In order to achieve meaningful applications, it is vital to increase the emission and photon extraction rates of color centers [16]. We can achieve increased emission rates by the well-known Purcell effect. The Purcell effect pertains to a field called cavity quantum electrodynamics (cavity QED, or CQED, for short). In this section, we review the fundamentals behind cavity QED, as well as its connections to later results presented in this thesis. We begin with a short recapitulation about photonic cavities, followed by an introduction to the strong and weak coupling regimes. Having developed this background, we conclude by providing a formal definition of the aforementioned Purcell enhancement.

2.2.1 Nanophotonic Resonators

While this thesis assumes the reader has a working understanding of resonators, for the sake of emphasis and clarity, we briefly review what is meant by the term “photonic resonator,” or “cavity.” These devices are one of the most fundamental ingredients in this research project, which is why it is critical to lay a common understanding about them. Broadly speaking, the function of a photonic resonator is to confine light spatially [44]. Photonic cavities are no different than any other kind of resonator in the field of physics: they are characterized by having eigenstates –or “modes”– with a time-harmonic evolution. For the purposes of this writing, all the formalism the reader might know about mechanical resonators applies to photonic resonators. The

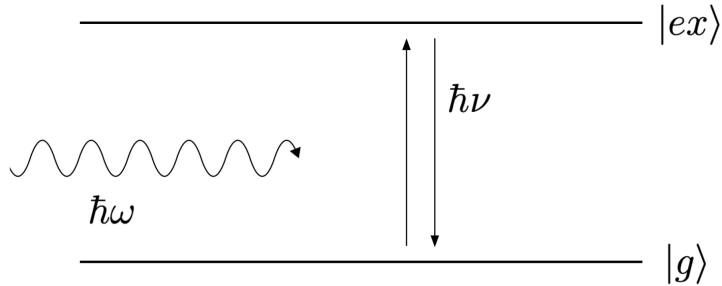


Figure 2.4: A generic two-level system

only intricacy is that, in the case of photonic resonators, modes take the form of solutions to Maxwell’s equations. That is, they are electromagnetic field distributions that satisfy Maxwell’s equations and are allowed to exist as long-lived states inside the cavity [45]. In this thesis, we are concerned with *nanophotonic* resonators, which confine light on length scales ranging from tens to hundreds of nanometers [44, 46]. Also known as nanocavities, these resonators have a wide array of applications, including nonlinear optics, biological sensing, chemical detection, and, most notably, quantum engineering [44]. In the preceding subsection, we study how photonic cavities can be used to manipulate quantum systems.

2.2.2 Cavity QED: the Strong and Weak Coupling Regimes

As its name suggests, cavity QED is concerned with the study of photonic resonators, and how these interact with light and quantum emitters. The most quintessential example of cavity QED is the single two-level emitter-resonator system. This is the physical situation that models the color center-photon dynamics. Given its paramount importance to this thesis, in this subsection, we will attempt to develop a formal understanding of it. Specifically, we will study its Hamiltonian, and use it to establish the physical regimes relevant to this research project.

Consider a two-level atom at \mathbf{r}_A with ground and excited states $|g\rangle$ and $|ex\rangle$, with dipole moment matrix elements $\mu_{ij} = \langle i|\mathbf{e}\mathbf{r}|j\rangle$, and raising and lowering operators $\hat{\sigma}_+ = |ex\rangle\langle g|$, $\hat{\sigma}_- = |g\rangle\langle ex|$, as shown in Fig. 2.4. The cavity has a field decay κ and the atomic dipole is characterized by a decay rate γ . The term κ represents the

decay rate of the cavity mode alone, whereas γ considers loss from all other modes and nonradiative decay routes. The total Hamiltonian of such a coupled quantum dot-cavity field system is described by the Jaynes-Cummings Hamiltonian,

$$\hat{H} = \hat{H}_A + \hat{H}_F + \hat{H}_{\text{int}}, \quad (2.1)$$

where the atomic Hamiltonian is given by

$$\hat{H}_A = \frac{\hbar\nu}{2}\hat{\sigma}_z, \quad (2.2)$$

the field Hamiltonian is

$$\hat{H}_F = \hbar\omega\left(\hat{a}^\dagger\hat{a} + \frac{1}{2}\right), \quad (2.3)$$

and the atom-field interaction Hamiltonian takes the form

$$\hat{H}_{\text{int}} = i\hbar(g^*(\mathbf{r}_A)\hat{a}^\dagger\hat{\sigma}_- - g(\mathbf{r}_A)\hat{\sigma}_+\hat{a}). \quad (2.4)$$

In this notation, \hat{a} and \hat{a}^\dagger represent the creation and annihilation operators, and $\hat{\sigma}_z = |ex\rangle\langle ex| - |g\rangle\langle g|$ is the population operator [47]. The term $g(\mathbf{r}_A)$ is the atom-field coupling parameter. For a classical field $\mathbf{E}(\mathbf{r})$ in a dielectric medium $\epsilon(\mathbf{r})$, the coupling parameter is defined as

$$g(\mathbf{r}_A) = \frac{\mu_{eg}}{\hbar} \sqrt{\frac{\hbar\omega}{2V_{\text{mod}} \max\{\epsilon(\mathbf{r})E^2(\mathbf{r})\}}} \hat{\mu}_{eg} \cdot \hat{e}E(\mathbf{r}_A), \quad (2.5)$$

where \hat{e} denotes the emitter orientation and V_{mod} is the mode volume of the cavity [47], given by the triple integral

$$V = \frac{1}{\max(\epsilon(\mathbf{r})E^2(\mathbf{r}))} \iiint d^3\mathbf{r} \cdot \epsilon(\mathbf{r})E^2(\mathbf{r}). \quad (2.6)$$

There is two scenarios we can identify based on the above coupling parameter. When the emitter-cavity coupling is stronger than the decay rates κ and γ (e.g., $|g(\mathbf{r}_A)| > \kappa, \gamma$), we say that we are in the strong coupling regime [47]. In the strong coupling regime, the two-level atom undergoes oscillations between the $|ex, n\rangle$ and

$|g, n + 1\rangle$ states, where $|ex, n\rangle$ is that excited atom state with n photons in the cavity, and $|g, n + 1\rangle$ is the ground state with $n + 1$ photons [47].

When the coupling parameter is smaller than the decay rates ($|g(\mathbf{r}_a)| < \kappa, \gamma$), we say that we are in the weak coupling regime [47]. In the weak coupling regime, irreversible spontaneous photon emission occurs due to dissipation. In vacuum, this spontaneous emission rate is given by the factor

$$\Gamma_0 = \frac{\mu_{eg}^2 \nu^3}{3\pi\epsilon_0 \hbar c^3}. \quad (2.7)$$

For a uniform dielectric medium with refractive index n , this expression translates to $\Gamma_n = n\Gamma_0$ [47]. As it was mentioned in this section's preamble, Γ_0 is limited for color centers. Because of this reason, we seek a method to enhance emission rates into the ZPL. This can be achieved via the Purcell effect, which we discuss next.

2.2.3 The Purcell Effect

It was in a brief abstract from 1946 that E.W. Purcell announced what would become one of his most notable discoveries. In *Proceedings of the American Physical Society*, the physicist noted that spontaneous emission rates could be increased (and decay times could be reduced) based on the environment of an atom [48]. Purcell discovered that, for an atom weakly coupled to a resonant device, the spontaneous emission probability was increased by the given factor

$$F_p = \frac{\Gamma}{\Gamma_n} = \frac{3Q\lambda^3}{4\pi^2 V n^3}, \quad (2.8)$$

where Q is the quality factor of the device, V is the aforementioned modal volume and λ is the resonant wavelength [48]. In layman terms, a quality factor a statement about the lifetime of a resonance. The larger the Q factor, the more time a mode takes to decay. It is also possible to think about quality factors in terms of the number of round trips light completes in a resonator before reaching a certain loss threshold [47]. Quality factors are a key figure of merit in this research project. Because of their importance, we dedicate the next few lines to their study.

2.2.4 The Quality Factor

To understand quality factors mathematically, we need to consider spectral features of a field coupled to a lossy resonator. In the presence of loss, the time-dependent electric field in the cavity takes the form

$$E(t) = E_0 e^{-\omega_0 t/2Q} e^{i\omega_0 t}. \quad (2.9)$$

In the above equation, $\kappa = \omega_0/2Q$ is the cavity field decay rate from earlier [47]. Fourier-transforming this time-decaying field, we can see that the spectrum is

$$E(\omega) = \int_0^\infty E_0 e^{-\omega_0 t/2Q} e^{i(\omega_0 - \omega)t} dt = \frac{E_0}{\omega_0/2Q - i(\omega_0 - \omega)}. \quad (2.10)$$

Incidentally, the squared magnitude of the field in frequency space becomes

$$|E(\omega)|^2 = \frac{|E_0|^2}{(\omega - \omega_0)^2 + (\omega_0/2Q)^2}, \quad (2.11)$$

which is a Lorentzian curve centered at ω_0 and with a FWHM of ω_0/Q [47]. Given a set of k modes with resonances ω_k 's, the spectrum of the resonator will be a collection of k Lorentzian peaks, and the lifetime of the k -th resonance will be determined by the Q -factor associated to the FWHM of said resonance [47].

Now that we understand all the relevant parameters in Eq. 2.8, let us step back for a moment. Take a second to revisit and appreciate Purcell's insight, for it is a truly remarkable property. In Eq. 2.8 lies the answer to a critical problem: the lacking extraction rate of color centers can be overcome by situating them in a long-lived (high Q), spatially confined (small V) resonance. Perhaps more concretely, the Purcell effect will occur if emitters are placed in cavity that is resonant at their ZPL [17]. A possible approach to meet this condition are Fabry-Pérot (FP) resonators, which we discuss next.

2.3 Fabry-Pérot Resonators

Because this thesis heavily uses FP resonators, in this section, we will study them extensively. We will discuss how to achieve high- Q resonances with these, and how to approximate their quality factors analytically.

2.3.1 The Resonance Condition in Fabry-Pérot Resonators

The premise underlying Fabry-Pérot resonators is straightforward. These devices confine light in the nanoscale by trapping it between two mirrors [49]. By tuning the distance between these reflectors, constructive interference inside the cavity can be achieved. This spatially confines light between the reflectors, and produces a standing wave mode [49].

The mirrors in FP cavities can take multiple forms, and can be realized in a wide multiplicity of ways. However, in solid-state systems, they are universally based on some modulation of the dielectric profile of the material [47, 50]. Photonic crystal resonators, for example, use the Bragg condition to reflect light at very high efficiencies [50]. For now, we will abstain from giving a very detailed account of the mirrors used in this thesis. A more in-depth discussion of the mirrors used for this writing will be provided in the methodology section.

The region where light is confined in the cavity is called the cavity length or spacer [47], and it is just as important as the mirrors. As foreshadowed in the previous paragraph, in order for resonant modes to be supported within the cavity, the standing-wave condition must be met. Thus, the spacer length must be a half-integer multiple of the wavelength in the material [49].

Naively, we would estimate the wavelength in the dielectric using the well-known result $\lambda = \lambda_0/n$. However, if we did this, we would likely find that our resonance peaks have shifted their expected locations in frequency space. Understanding this mismatch requires us to consider the physics of an electromagnetic wave travelling through a dielectric with a finite cross-sectional area.

When a plane wave is propagating along a waveguide, the mode is not fully contained in the dielectric; its tails are traversing the cladding region. We can account

for this nuance –for the spreading of mode out of the waveguide– with the effective index approximation [47]. In this approximation, we treat modes as a plane wave propagating through a homogeneous medium with refractive index n_{eff} , where

$$n_{\text{eff}}^2 = n^2 b + n_0^2 (1 - b). \quad (2.12)$$

In the above, n is the refractive index of the waveguide, n_0 is the refractive index of the cladding material, and b is the field confinement factor, which is approximately defined as

$$b \approx 1 - \frac{2 \ln(1 + \nu^2/2)}{\nu^2}. \quad (2.13)$$

For a waveguide of thickness d , ν , which is just the normalized frequency, is given by

$$\nu = \frac{2\pi}{\lambda} d \sqrt{n^2 - n_0^2}. \quad (2.14)$$

All this is to say that, when designing our resonator, we should keep into account that the spacer must be designed for wavelengths λ/n_{eff} [47]. The naive, usual λ/n might fail to accurately predict the location of our resonant modes.

2.3.2 Calculating Q -Factors in Fabry-Pérot Resonators

Having a theoretical, formal understanding of Q -factors, and knowing how to estimate these, will become an essential skill in our toolbox later in this thesis. We thus proceed by proving a method to approximate quality factors in an FP cavity analytically.

After one full round-trip, the energy in a resonator decays as

$$W(\tau) = W_0 e^{-2\alpha L} R_1 R_2, \quad (2.15)$$

where α is the absorption loss per unit length of the cavity length, L is the length of the spacer, and R_1 and R_2 are the reflectivities of the mirrors [47]. The greek letter τ is the round-trip across the resonator, and it is roughly given by

$$\tau \approx \frac{2n_{\text{eff}}L}{c}. \quad (2.16)$$

From the discussion in the previous subsection, we can conclude that

$$W(t) = W_0 e^{-\omega_0 t/Q}. \quad (2.17)$$

Combining equations 2.11 and 2.13 and solving for Q , we obtain

$$Q \approx \frac{\omega n_{\text{eff}}}{c \left(\alpha - \frac{1}{L} \ln \sqrt{R_1 R_2} \right)}. \quad (2.18)$$

As we can see, in order to maximize the quality factor, we are interested in having mirrors with an efficiency as close to unity as possible. Furthermore, we also require a mode that is well-confined in the dielectric (in other words, maximize n_{eff}) [47]. These observations will inform our choice of parameters later in this writing. Now, having developed such an extensive discussion on how resonators work –both classically and in the quantum regime, we are finally able to discuss the mirrors employed in this research project. These were optimized using a technique known as photonic inverse design, and simulated using the finite-difference time-domain method. In the proceeding section, we provide an overview of these two computational techniques.

2.4 Electromagnetic Simulation and Inverse Design

This thesis is, for the most part, of a theoretical nature. While we are proposing a technology for practical applications, we are focusing on providing a rigorous treatment and analysis of said technology. Because of the geometrical complexity of the structures we are studying, there is no way to model them analytically [50]. Solving Maxwell's equations for a structure like the one shown in Fig. 2.5 would be an extremely difficult process. Because of this reason, we study these devices through numerical simulations. Electromagnetic simulation lies at the heart of this research

project, and is also key to inverse design protocols, which employ these heavily in their optimization routines [51]. In this section, we overview the foundational principles of electromagnetic simulations solvers. Having established this background, we introduce the inverse design method.

2.4.1 The Finite-Difference Time-Domain Method

The finite-difference time-domain (FDTD) method is one of the most-widely used simulation techniques in the field of photonics. As it has been already mentioned, this is the framework that was used in our inverse design routines. It was also the framework we used to simulate the performance of our resulting devices. In a nutshell, this protocol is based on the spatial discretization of dielectric structures [52]. Given an electromagnetic source, which is specified by the user based on the type of problem in question, FDTD algorithms solve Maxwell's equations for that source over a temporal-spatial grid using central-difference approximations [52]. This allows the user to retrieve the time evolution of the fields in the structure of interest.

2.4.2 Inverse Design

In recent years, we have been witnesses to incredible advances in the fields of optimization and computation [19, 20]. Borrowing from the principles of machine learning, we have achieved unprecedented progress in computer vision, natural language processing, and many other branches of computer science. The field of photonics has not remained elusive to these breakthroughs. Inverse design, a set of algorithmic techniques for optimizing photonic structures based on client-specified functionalities, has gained increasing momentum over the past ten years, leading to unprecedented developments across a wide range of photonic applications [19, 20].

Traditionally, the design of nanophotonic devices has been founded upon the application of a priori knowledge of physical effects [19]. Under traditional approaches, designers fine-tune a limited repertoire of geometrical parameters to optimize device performance for a given target wavelength and material [19]. While these traditional methods have led to remarkable technological advancements in the past two decades

[45], for several design problems, intuition-driven design does not provide any clear approach to follow [20]. Furthermore, given the restricted parameter space of traditional design libraries, it is unclear whether optimal performance can truly be achieved with these [19].

Inverse design algorithms provide an automated protocol for device design, and have been repeatedly used to produce non-intuitive devices with a superior performance and new functionalities relative to their traditional counterparts [19]. Rather than optimizing a small set of parameters based on electromagnetic first principles, inverse design algorithms parameterize the entire design space of the optimization region, thereby exploring a significantly larger design space [51, 53]. Under a typical inverse design scheme, the user specifies a design area, a wavelength of interest, a dielectric constant, and a desired functionality. The algorithm will output a geometry at the required wavelength and dielectric constant that optimizes performance relative to the user-specified functionality [19, 20]. Beyond automated design and the possibility of improved performance, inverse design schemes allow users to specify minimal feature sizes [54], which has important implications in fabrication scalability and performance reliability.

In general, inverse design algorithms optimize devices by computing the gradient of a function the user seeks to minimize, called the objective function [51]. While evaluating the gradient relative to dielectric changes in a structure may sound like an intractable problem, it is actually a solvable one. The key to this problem lies in the adjoint method, which is extensively explained by L.W. Su (2020), in Ref. [51]. While the details of the adjoint method are beyond the scope of this research project, there are two key elements of it that are relevant to us. First and foremost, it requires reliable simulations of electromagnetic fields in order to compute the gradient of the objective function [51]. These simulations are oftentimes performed via the FDTD algorithm [51]. Secondly, it is worthwhile mentioning that the adjoint method was used by the inverse design routines employed for this thesis [51].

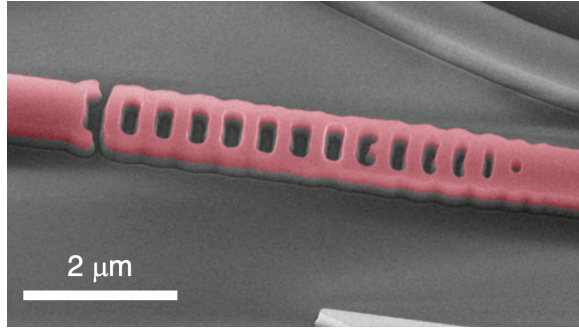


Figure 2.5: An inverse-designed reflector

2.4.3 Made in Spilker: Prior Work on Inverse-Designed Mirrors

There is already an extensive lineage of inverse-designed FP resonators in the Vučković group. This proud tradition of devices traces itself back to 2022, when Ahn et al. proposed these as a platform for solving resonant problems with inverse design [55]. Historically, resonant devices had remained challenging to inverse design methodologies due to their highly nonconvex parameter spaces [56]. Because inverse design protocols are so heavily reliant on gradient descent, optimizing functions with non-uniform curvatures is remarkably challenging. There is a non-trivial risk of converging to local minima, which would severely hinder the performance of resulting devices [55].

In a paper published in *ACS Photonics*, researchers from the lab argued that this issue could be overcome by mapping resonant devices to a set of nonresonant problems [55]. By optimizing highly reflective mirror structures and using these to make FP cavities, Ahn et al. were able to achieve flexible dispersion engineering, as well quality factors exceeding two million on a silicon-on-insulator platform [55]. In subsequent work, Yang et al. (2023) used inverse-designed silicon-carbide FP resonators to demonstrate quantum and classical nonlinear light generation (Fig. 2.5), furthering the potential of inverse design schemes to optimize nanophotonic resonators [21].

Based on the ability to enforce minimal feature sizes and its unparalleled scalability, inverse design protocols host vast potential for applications in cavity QED with

color centers. Up until recently, however, the integration of inverse design and diamond cavity QED remained an outstanding challenge due to limitations in processing and fabrication [19, 57]. Because diamond is hard to process and was available only in bulk form on small chips, fabrication was highly volatile and intricate. Established processing techniques, such as quasi-isotropic etching, severely limited the range of fabricable device geometries and imposed large minimal feature sizes [58]. This made diamond poorly-suited for inverse design implementations. The recent development of diamond-on-insulator thin-films has lifted these constraints, allowing for scalable diamond fabrication, as well as for integration with coherent diamond qubits [58]. The present work builds on this breakthrough, seizing it to exploit the promises of inverse design for applications with diamond color centers.

2.5 Chapter Summary

In this chapter, we learned about the importance of quantum networks. While these are still not a commercially-available technology, they promise to realize a myriad of exciting applications, including quantum key distribution, quantum simulation, and distributed quantum computing. We argued that color centers held vast potential for applications in quantum networks due to their exquisite properties. In particular, the tin-vacancy center stood out based on its high quantum efficiency and reduced phonon absorption rates at 1.7 K, as well as the absence of first order Stark shift, facilitating its integration in devices and increasing its robustness to any interfaces and charge fluctuations.

We noted that an important limitation of color centers was their limited photon extraction rates in bulk. We can easily overcome this limitation via the Purcell effect. Purcell enhancements can be achieved by situating these emitters in Fabry-Pérot cavities, which we will optimize using inverse design techniques. Inverse design, if used for cavity QED with color centers, could have important implications in the scalability and optimization of quantum node architectures. However, up to date, the integration of inverse design techniques with diamond cavity QED has remained an outstanding challenge due to limitations in processing and fabrication. The advent

on diamond thin-films now allows for the full potential of inverse design. Based on this recent breakthrough, this thesis seeks to establish a theoretical framework for the future unification of inverse design photonics and cavity QED with color center defects.

Chapter 3

Mirror Design and Optimization

As explained in Chapter 2, the primary goal of this thesis is to employ inverse design algorithms to optimize diamond nanophotonic resonators for cavity QED with tin vacancy centers. Due to the non-convex parameter landscape of Q factors, it is strategic to begin by solely focusing on optimizing high-performance mirrors. If we can devise a highly reflective structure at $\lambda_{\text{ZPL}} = 620$ nm, in order to deterministically achieve long-lived resonances at the SnV^- ZPL, all that is left to do is to appropriately select a spacer length. This can be done while satisfying stringent fabrication constraints for diamond (such as large features), via constrained optimization. In this chapter, we will detail how our diamond nanophotonic mirrors were optimized. We will explore the key ingredients of our design recipe, and discuss the performance of our resulting devices. In later chapters, we will integrate these reflectors into a complete resonant system.

3.1 Inverse-Design Problem Formulation

Having established the computational resources and framework that we used to optimize our devices, we can now address our problem set-up, and discuss the parameters that were used in our design scheme. *How did we optimize our reflectors?* In the upcoming sections, we answer this question. We formulate our inverse design problem using the scattering matrix formalism, and enforce dimensional constraints on

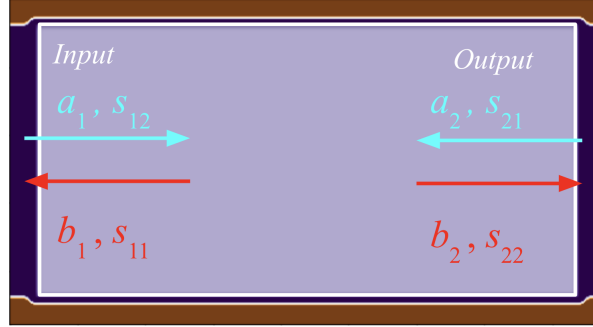


Figure 3.1: Physical setup for a generic scattering matrix

our devices based on our knowledge about photonics and waveguide systems.

3.1.1 The Scattering Matrix

In order to optimize our reflectors, we seek to minimize the overlap between some input and output regions in a diamond waveguide, as shown schematically in Fig 3.1. This can be done by maximizing the diagonal matrix of the scattering matrix, \mathbf{S} , for this process [59]. For instance, to make a reflector that maximizes the overlap between the amplitudes a_1 and b_1 in Fig. 3.1, an optimizer that maximizes \mathbf{S}_{11} is desired [59].

Also known as the S -matrix, the scattering matrix is of crucial importance in several fields across physics, including quantum mechanics, quantum field theory, high-energy physics, and photonics [60]. All this matrix does is to relate the initial and final states of a system following a scattering process [59]. Formally, for the structure shown in Fig. 3.1, the scattering matrix would take the form

$$\mathbf{S} = \begin{bmatrix} s_{11} & s_{12} \\ s_{21} & s_{22} \end{bmatrix}, \quad (3.1)$$

where s_{11} and s_{12} denote the input's reflection and transmission coefficients, and, by analogy, s_{21} and s_{22} denote the output's reflection and transmission coefficients [59].

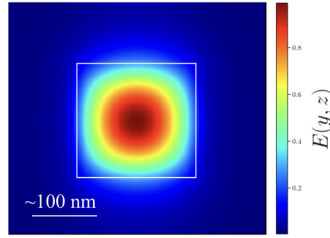


Figure 3.2: An electric field inside a diamond waveguide

3.1.2 Constraining Waveguide Dimensions

In photonics design, a relevant constraint to consider is the physical dimensions of the system to be optimized. It is likely intuitive to the reader that, for any arbitrary application requiring a wavelength of size λ , we would like a device with physical dimensions on the order of λ . This intuition explains why microwave ovens are roughly the size of shoe box (that is the size of a 30 cm wavelength), or why fiber optics have such tiny diameters (that is the size of telecom waves).

While it may be tempting for us to naively design a square $620 \times 620 \text{ nm}^2$ waveguide, in the spirit of scientific discipline and rigor, we will (and need to) be somewhat more pedantic than that. In particular, it is critical that we ensure that only the fundamental mode is supported by our host waveguide. The presence of high-order modes can lead to coupling between distinct mode families, which can be hugely detrimental to device performance [55].

Multimode behavior would make our simulations intractable, preventing us from efficiently simulating transmission measurements and making it nearly impossible to isolate high- Q resonances. We can prevent these issues by restricting our devices to waveguides with a cross-sectional area below $300 \times 300 \text{ nm}^2$. Under this threshold, only the fundamental mode is supported, and multimode behavior is not a concern.

For electromagnetic waves propagating along a waveguide, there are two kinds of modes we need to consider. The first kind are so called TE (transverse-electric) modes [61]. For TE modes, the electric field is transverse to the direction of propagation [61]. For TM (transverse-magnetic) modes, by contrast, the magnetic field is transverse to the direction of propagation [61].

Fig. 3.2 shows a cross-sectional cut of the electric field distribution within a square $200 \times 200 \text{ nm}^2$ diamond waveguide for a TE-like mode with $\lambda_{\text{ZPL}} = 620 \text{ nm}$, simulated with *fdtd-z*, SPINS Photonics’ open-source FDTD simulation engine. As we can see, for these waveguide dimensions, the field distribution is well-confined inside the dielectric, and is maximized at the center of the structure. Based on these features, we confirm that we have realized a single-mode device, which we proceed to optimize.

3.2 Inverse-Designed Reflectors

Having confirmed that we have designed a diamond waveguide that supports a single mode at $\lambda_{\text{ZPL}} = 620 \text{ nm}$, in this section, we input this waveguide into an inverse design routine. We optimize a mirror with near-unity reflectivity, and design a FDTD simulation to study the performance of our resulting device.

3.2.1 Optimization Recipe

As previously mentioned, the low-level nuances of the inverse design algorithm are outside the scope of this thesis. However, leaving these details aside does not prevent us from developing a high-level understanding of our optimization routine. Because the steps in these routines can have an important effect on the performance and geometry of resulting devices, in this sub-section, we briefly outline the optimization protocol used in this thesis. On a high-level, the inverse design routine employed here is straightforward.

We begin by defining a design region in our waveguide from the previous section. We do this by setting the dielectric in said inner region to $\epsilon_{\text{avg}} = (\epsilon_{\text{Dia}} + \epsilon_0)/2$, where ϵ_{Dia} denotes the permittivity of diamond (see top schematic in Fig. 3.3). After enforcing minimal feature size constraints, we proceed to run a free-form optimization routine. In this step, the inverse design algorithm explores a continuous distribution of permittivities between ϵ_0 and ϵ_{Dia} . It renders an optimized device, with a design region of continuous values between ϵ_0 and ϵ_{Dia} , as shown pictorially in the middle

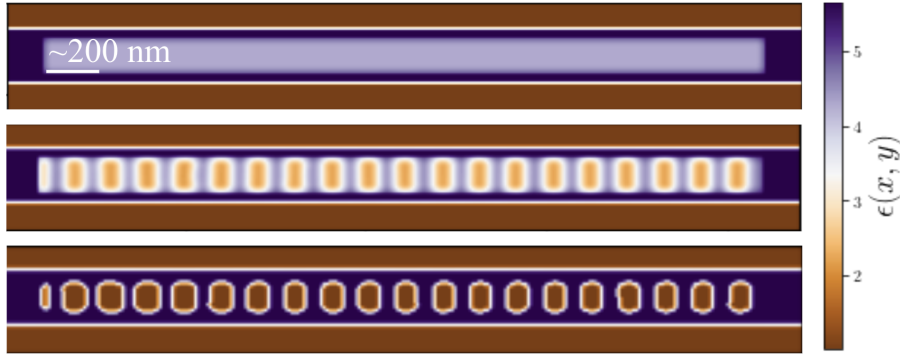


Figure 3.3: Inverse-design optimization of a single mirror

plot of Fig. 3.3.

For practical applications, fabricating a device with a continuous dielectric profile is impossible. Because of this reason, we need to discretize the resulting structure. In the binarization step of our optimization routine, we discretize the optimized mirror by defining a threshold dielectric constant, $\epsilon_{\text{threshold}}$. Values of the continuous permittivity above $\epsilon_{\text{threshold}}$ are set to ϵ_{Dia} , and values below $\epsilon_{\text{threshold}}$ are set to ϵ_0 . In the last step of our protocol, a final optimization routine enforces minimal feature sizes, which are determined by fabrication considerations. Based on the group’s current nanofabrication capabilities, we enforced a minimal feature size radius of 100 nm. The bottom plot of Fig. 3.3 shows the final device¹.

3.2.2 Testing Mirror Performance

We confirm the success of our inverse design optimization routine by running a full transmission simulation of our resulting mirror. We do this by implementing a three-dimensional FDTD simulation using Ansys’ Lumerical, one of the most widely-used photonics simulation engines across both industry and academia. For all practical matters, this simulation can be seen as a numerical trial, intended to predict the results we would obtain in a perfectly ideal laboratory experiment. The simulation

¹This is not the device studied in subsequent sections; it is a smaller reflector, which is easier to visualize in the limited size of a figure. The mirrors we will study in this thesis are longer (at 9.4 μm), as shown in Fig. 3.4. We chose these longer mirrors based on their increased reflectivities.



Figure 3.4: Transmission simulation set-up

setup, shown pictorially in Fig. 3.4, consisted of four key elements: (i) a mode source set to 620 nm (schematically represented as a purple arrow), (ii) a 3-microns-long diamond waveguide (cross sectional area of $200 \times 200 \text{ nm}^2$), (iii) our inverse-designed reflector, and (iv) a simulation environment.

The simulation environment, which determines the computational parameters of the FDTD routine, was set at a mesh accuracy of four, which corresponds to 18 mesh points per wavelength. At this resolution, a good trade-off between simulation accuracy and the memory costs of fine spatial discretization is achieved [50].

The boundary conditions used for the simulation were perfectly-matched layers (PMLs), shown in orange. PMLs are a class of boundary conditions meant to absorb incident light with minimal reflection. These are a critical component to non-periodic electrodynamics simulation, for they prevent computational anomalies due to interference effects from waves reflected at the simulation boundary [50]. PMLs were placed approximately a wavelength away from the vacuum-diamond interface.

In general, simulating the behavior of resonant devices requires long computation times. As it will be explained later on, this is because fields take substantial amount of time to decay when coupled to cavity systems. Thus, to faithfully calculate their time-evolution, long simulations are required. Because no resonant behavior was being simulated yet, we were able to enforce a relatively short computation time (330 fs) without compromising simulation accuracy.

In order to probe the response of our reflector over a large frequency regime, we set the mode source bandwidth to 80 nm. To prevent interference abnormalities due to counter-propagating waves at the waveguide-reflector boundary, rather than measuring reflectance by collecting from behind the source, we added a two-dimensional

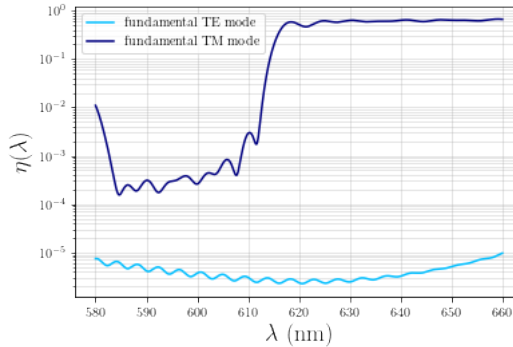


Figure 3.5: Simulated reflector performance

transmission monitor at the mirror’s output (see yellow screen in Fig. 3.4). We simulated two source polarizations: TE and TM. The spectra for these are shown in Fig. 3.5. As we can see, for the TE source, our reflector behaves as a near-perfect mirror for all pulses between 580 and 660 nm. Its performance for the TM source is, in comparison, significantly deprecated, with transmission coefficients exceeding 10^{-1} near the SnV⁻ ZPL. This is a perfectly reasonable result: all it tells us is that our inverse design routine optimized for a TE source. Based on this insight, we set ourselves to simulate and optimize TE sources for the remainder of this thesis.

3.3 Chapter Summary

In this chapter, we formulated our inverse design problem through a scattering matrix argument. In particular, we determined that, in order to optimize our reflectors, we had to maximize the diagonal components of the scattering matrix representing our waveguide-mirror system. We used this argument to design our mirrors. Based on FDTD simulations, we found that our inverse design routine had achieved a near-perfect mirror for the fundamental TE-like mode of a $200 \times 200 \text{ nm}^2$ suspended diamond waveguide.

Chapter 4

An Inverse-Designed Fabry-Pérot Resonator

Armed with our inverse-designed reflectors, we can proceed to optimize a full FP resonator. As formerly implied, the transition from a single reflector to a FP cavity is straightforward: we must produce a mirror copy of some reflector, and “stack” the two resulting devices against each other. In this chapter, we will provide a detailed analysis of our resulting nanocavities. By optimizing the spacing between our inverse-designed mirrors, we will fine-tune these cavities to achieve resonances near the SnV^- ZPL. We will systematically study the properties of our microresonators, using the principles of cavity QED to assess whether these are suitable for applications with quantum emitters.

4.1 Simulating High- Q Resonators

Because this thesis is of a theoretical nature, in order to determine the Q factors of our devices, we need to set up an appropriate simulation. Setting up Q -factor simulations is a non-trivial task. There are multiple intricacies that must be taken into account, including the need for appropriate simulation boundary conditions, simulation time, and several other parameters. To make sure we address all these

numerous intricacies correctly, in the preceding section, we dive deep into the Q -factor simulation used for this thesis.

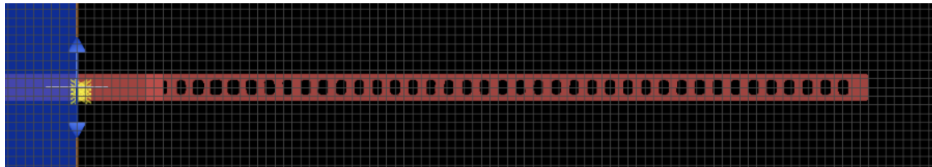
4.1.1 Optimizing Emitter Location

Based on Eq. 2.4, we know that, in order to maximize the interaction term of the cavity-atom Hamiltonian, we must maximize the magnitude of the field experienced by the emitter. Recalling this information, we situate a dipole emitter at the very center of the simulation environment, where we heuristically expect to find the largest fields (see Fig. 4.1). This dipole emitter will serve the role of a source in our upcoming Q -factor simulations.

4.1.2 Simulation Setup

Just as earlier, to calculate the quality factor of our inverse-designed reflectors, we set up a 3D FDTD simulation in Lumerical (Fig. 4.1). As with our spectra simulations, we use a mesh accuracy of four. Lumerical has build-in functions to calculate quality factors (called Qanalysis objects). We add one of these to the center of the simulation environment (see yellow crosses), where we expect the field magnitudes to be maximal. Because Qanalysis objects calculate Q -factors by taking the Fourier transform of the field decay, we need to make sure we run the simulation for a sufficiently long time—long enough for Lumerical to extract a decay envelope. We thus set the simulation time to 2000 fs. In order to avoid multimode behaviour, a narrow pulse bandwidth (20 THz) was chosen.

We set all boundary conditions to PMLs, making sure these are at least a wavelength away from the diamond-vacuum interface. Resonant simulations tend to be computationally costly due to their long run times. To ease this computational burden, we enforce symmetric boundary conditions about the center of the cavity (see blue shaded region in Fig. 4.1). Enforcing this symmetry effectively reduces the simulation volume by a factor of two. Because the fields on one side of the simulation can be directly extracted by mirroring the field solutions on the opposite side, we can get discard half of the simulation space. For an FDTD simulation of volume V

Figure 4.1: Q -factor simulation setup

and a grid size of δx , simulation time scales as $\sim V\delta x^{-4}$ [50], which means that the appropriate use of symmetry can make calculations extremely more efficient.

4.2 Resonator Optimization

With a fully-operational Q factor FDTD simulation, we can now perform one of the most critical tasks in this thesis: putting it all together into a functioning diamond cavity, fined-tuned to enhance the emission of a tin-vacancy emitter sitting at its center. In the upcoming section, we optimize our diamond microcavities and study their resonant behavior. In particular, we determine their quality factors and Purcell enhancements, key figures of merit behind this research project.

4.2.1 Spacer Sweeping

We have finally gathered all the simulations and knowledge needed to optimize the spacer of our resonators. Now, we can determine whether the devices we have been studying so extensively can support long-lived modes. In what some might rightfully call a brute-force approach, we sweep the length of our cavity spacer from 0 to 2 μm , hoping (or, more accurately, making an educated guess) that resonances will be supported somewhere in this regime. Our results are shown in Fig. 4.2.

As predicted by theory [62], we observe a collection of successive, equally-spaced resonant peaks, which correspond to the intervals over which the standing wave condition is met, and FP modes can be supported. We note that the width of these intervals increases as a function of L . This observation is consistent with the intuition that longer devices support a decreased free spectral range.

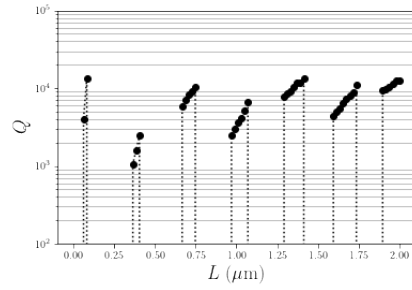


Figure 4.2: Q -factors of resulting devices

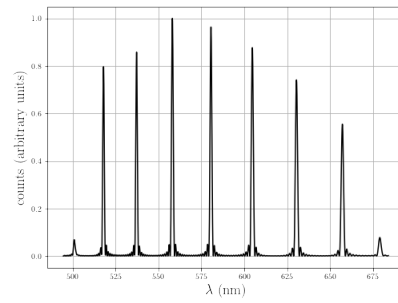


Figure 4.3: Inverse-designed resonator spectrum for $L = 5 \mu\text{m}$

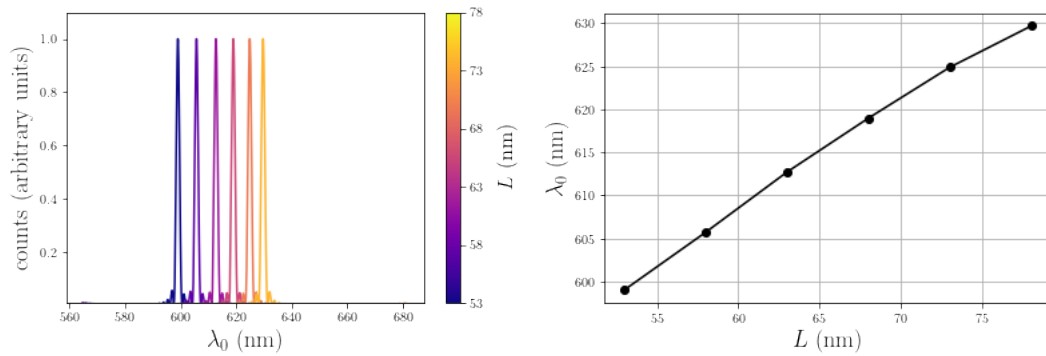


Figure 4.4: Resonant modes in our FP resonators

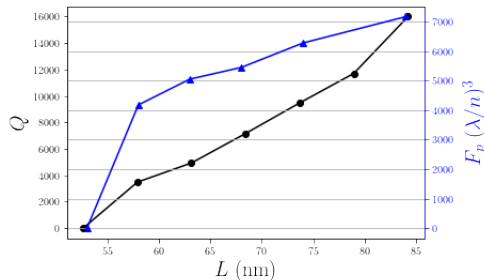


Figure 4.5: Purcell enhancement of resulting devices

Fig. 4.4 shows the modes of our resulting devices for different spacer values. As we can see, tuning the cavity length to 70 nm leads to a resonant mode near the SnV⁻ ZPL. This is a perfectly reasonable result. Using Eq. 2.12, we estimate the effective index of our spacer at $n_{\text{eff}} \approx 2.16$. Based on this approximation, the wavelength in the dielectric should be $\lambda = \lambda_0/n_{\text{eff}} \approx 287$ nm. Thus, a cavity spacer of 70 nm corresponds to, approximately, to a quarter of a wavelength. Physically, this suggests we are looking at a well-confined mode, with a field concentrated in the high-index region of the resonator.

Looking at Fig. 4.4, we note that the resonances vary approximately linearly with the size of the spacer. This is to be expected: intuitively, in the resonant regime, we should expect a scaling in the gap by k to increase the wavelength as $k\lambda$. As we can see in Fig. 4.4, through very precise tuning of the cavity spacing, we can achieve remarkably fine control over the device’s resonant wavelength.

4.2.2 Purcell Enhancement of Resulting Devices

In Fig. 4.2 and in Fig. 4.5, we observe high-quality resonances over the regime $L \in (55, 90)$ nm. The Q -factor is maximized for a gap of 83 nm. As we tune the spacer size to resonance, constructive interference starts taking place within the resonator, allowing for a standing-wave mode. Our modal volumes, which we calculated to be on the order of $10^{-3} \mu\text{m}^3$, are consistent with prior works using similar resonators in this frequency regime [16, 17]. Using the analytical model derived in Chapter 2 (Eq. 2.18), we find our simulated Q factors to be in strong agreement with theory. For

$\omega \approx 485/(2\pi)$ THz, the reflectances from Chapter 3, and assuming $\alpha=0$, we obtain $Q \sim 3 \times 10^4$, which is consistent with our simulations. In Fig. 4.5, we also show the Purcell enhancement and quality factor of our devices as function of L in the range from 50 to 85 nm. We calculated these enhancements using Eq. 2.8. We consistently observe enhancements exceeding $10^3 (\lambda/n)^3$. Based on literature, we find this range suitable for applications in quantum communications and sensing [15, 17, 18]. In fact, for this range of Purcell factors, it is expected that color centers in resonators would already enter the regime of strong coupling and exhibit light-matter entanglement.

4.3 Chapter Summary

In this chapter, we successfully turned our inverse-designed mirrors into fully functional nanophotonic resonators. We saw that our resulting devices were in robust agreement with theoretical predictions for FP resonators. By optimizing the size of the spacer region, we achieved high- Q resonances and small modal volumes at the tin-vacancy ZPL. Having Purcell factors exceeding 10^3 , these microresonators should strongly couple emitters to the cavity mode, which makes them ideal for applications in QST.

Chapter 5

Summary and Outlook

In this thesis, we optimized FP nanophotonic resonators for applications in cavity QED. Photonic cavities hold vast potential for numerous quantum information technologies, including metrology, computing, and simulation. These cavities allow for precise control of the quantum-mechanical properties of solid-state electronic spin states, and are key ingredients for the realization of coherent light-matter interfaces.

Group-IV color centers have emerged as prime candidates for quantum networks based on their long coherences and potential for integration in nanophotonics. These emitters are a central topic of research in the Vučković lab. In this thesis, we focused on the tin-vacancy center, which has been extensively studied by the group.

Using the latest developments in inverse design capabilities, we optimized mirrors with near-zero transmission loss at the SnV⁻ ZPL. These mirrors were used to produce FP resonators with quality factors exceeding 10^4 . We found resonances with modal volumes on the order of $10^{-2} \mu\text{m}^{-6}$. These modal volumes and Q -factors implied Purcell enhancements on the order of 10^3 . Based on literature, we found these enhancements suitable for applications in quantum communication and sensing.

To the best of our knowledge, these results constitute the first theoretical study of inverse design for cavity QED with tin-vacancy defects. The work presented herein paves the way for the experimental integration of color centers with inverse-designed nanophotonic resonators. Thanks to the development of diamond thin-films, inverse design has become a suitable platform for the optimization of nanophotonic diamond

devices. Thus, the integration of thin-film diamond with inverse design could have major implications in the scalability of solid-state quantum network architectures.

There are several possible avenues to extent this research. For example, it is of interest to optimize diamond-on-insulator devices. Optimizing nanostructures on a diamond-on-insulator platform would lift the requirement of fully-connected devices, significantly broadening design space. Similarly, it remains to determine whether our quality factors can be further optimized. Based on Eq. 2.18, increasing the spacer length should lead to larger quality factors. However, longer spaces also lead to larger modal volumes, which imply a less confined mode, and may degrade Purcell enhancement. It would be interesting to see how this trade-off between larger quality factors and larger modal volumes would impact device performance.

Alternatively, it might be possible to optimize mirrors that selectively reflect the spacer's fundamental mode. Previous works have used this approach to make high-quality resonators. By transmitting higher-order modes, devices designed in this way avoid multimode behavior, while being allowed to possess larger cross-sectional areas that minimize scattering losses over the resonator's length.

Bibliography

- [1] Sara L. (Sara Lambert) Mouradian. *A scalable quantum computation platform: solid state quantum memories coupled to photonic integrated circuits*. Thesis, Massachusetts Institute of Technology, 2018.
- [2] M.T. Ruf. *Cavity-enhanced quantum network nodes in diamond*. Dissertation (TU Delft), 2021. ISBN: 9789085934837.
- [3] Eleanor Rieffel and Wolfgang Polak. *Quantum computing: a gentle introduction*. Scientific and engineering computation. The MIT Press, Cambridge, Mass, 2011.
- [4] S. Pirandola, B. R. Bardhan, T. Gehring, C. Weedbrook, and S. Lloyd. Advances in photonic quantum sensing. *Nature Photonics*, 12(12):724–733, December 2018. Publisher: Nature Publishing Group.
- [5] Nicolas Gisin and Rob Thew. Quantum communication. *Nature Photonics*, 1(3):165–171, March 2007. Publisher: Nature Publishing Group.
- [6] Ke Bian, Wentian Zheng, Xianzhe Zeng, Xiakun Chen, Rainer Stöhr, Andrej Denisenko, Sen Yang, Jörg Wrachtrup, and Ying Jiang. Nanoscale electric-field imaging based on a quantum sensor and its charge-state control under ambient condition. *Nature Communications*, 12(1):2457, April 2021. Publisher: Nature Publishing Group.
- [7] Zhengzhi Jiang, Hongbing Cai, Robert Cernansky, Xiaogang Liu, and Weibo Gao. Quantum sensing of radio-frequency signal with NV centers in SiC. *Science Advances*, 9(20), May 2023. Publisher: American Association for the Advancement of Science.

- [8] Vinayak V. Dixit and Chence Niu. Quantum computing for transport network design problems. *Scientific Reports*, 13(1):12267, July 2023. Publisher: Nature Publishing Group.
- [9] T. D. Ladd, F. Jelezko, R. Laflamme, Y. Nakamura, C. Monroe, and J. L. O’Brien. Quantum computers. *Nature*, 464(7285):45–53, March 2010. Publisher: Nature Publishing Group.
- [10] 40 years of quantum computing. *Nature Reviews Physics*, 4(1):1–1, January 2022. Publisher: Nature Publishing Group.
- [11] Valentin Gebhart, Raffaele Santagati, Antonio Andrea Gentile, Erik M. Gauger, David Craig, Natalia Ares, Leonardo Bianchi, Florian Marquardt, Luca Pezzè, and Cristian Bonato. Learning quantum systems. *Nature Reviews Physics*, 5(3):141–156, March 2023. Publisher: Nature Publishing Group.
- [12] Francesco Bova, Avi Goldfarb, and Roger Melko. Quantum Computing Is Coming. What Can It Do? *Harvard Business Review*, July 2021. Section: Innovation.
- [13] Quantum technology is beginning to come into its own. *The Economist*.
- [14] Christophe Couteau, Stefanie Barz, Thomas Durt, Thomas Gerrits, Jan Huwer, Robert Prevedel, John Rarity, Andrew Shields, and Gregor Weihs. Applications of single photons to quantum communication and computing. *Nature Reviews Physics*, 5(6):326–338, June 2023. Publisher: Nature Publishing Group.
- [15] Maximilian Ruf, Noel H. Wan, Hyeonrak Choi, Dirk Englund, and Ronald Hanson. Quantum networks based on color centers in diamond. *Journal of Applied Physics*, 130(7):070901, August 2021. Publisher: American Institute of Physics.
- [16] Alison Emiko Rugar, Jelena Vuckovic, Nicholas A. Melosh, and Zhi-Xun Shen. *Quantum photonics with the tin-vacancy center in diamond*. PhD thesis, Stanford University, Stanford, California, 2022.

- [17] Alison E. Rugar, Shahriar Aghaeimeibodi, Daniel Riedel, Constantin Dory, Haiyu Lu, Patrick J. McQuade, Zhi-Xun Shen, Nicholas A. Melosh, and Jelena Vučković. A Quantum Photonic Interface for Tin-Vacancy Centers in Diamond. *Physical Review X*, 11(3):031021, July 2021. arXiv: 2102.11852.
- [18] Julian M. Bopp, Matthias Plock, Tim Turan, Gregor Pieplow, Sven Burger, and Tim Schröder. Sawfish Photonic Crystal Cavity for Near-Unity Emitter-to-Fiber Interfacing in Quantum Network Applications, October 2022.
- [19] Constantin Dory, Dries Verdecruysse, Ki Youl Yang, Neil V. Sapra, Alison E. Rugar, Shuo Sun, Daniil M. Lukin, Alexander Y. Piggott, Jingyuan L. Zhang, Marina Radulaski, Konstantinos G. Lagoudakis, Logan Su, and Jelena Vučković. Inverse-designed diamond photonics. *Nature Communications*, 10(1):3309, July 2019.
- [20] Sean Molesky, Zin Lin, Alexander Y. Piggott, Weiliang Jin, Jelena Vucković, and Alejandro W. Rodriguez. Inverse design in nanophotonics. *Nature Photonics*, 12(11):659–670, November 2018.
- [21] Joshua Yang, Melissa A. Guidry, Daniil M. Lukin, Kiyoul Yang, and Jelena Vučković. Inverse-designed Silicon Carbide Quantum and Nonlinear Photonics, March 2023.
- [22] Frank Arute, Kunal Arya, Ryan Babbush, Dave Bacon, Joseph C. Bardin, Rami Barends, Rupak Biswas, Sergio Boixo, Fernando G. S. L. Brandao, David A. Buell, Brian Burkett, Yu Chen, Zijun Chen, Ben Chiaro, Roberto Collins, William Courtney, Andrew Dunsworth, Edward Farhi, Brooks Foxen, Austin Fowler, Craig Gidney, Marissa Giustina, Rob Graff, Keith Guerin, Steve Habegger, Matthew P. Harrigan, Michael J. Hartmann, Alan Ho, Markus Hoffmann, Trent Huang, Travis S. Humble, Sergei V. Isakov, Evan Jeffrey, Zhang Jiang, Dvir Kafri, Kostyantyn Kechedzhi, Julian Kelly, Paul V. Klimov, Sergey Knysh, Alexander Korotkov, Fedor Kostritsa, David Landhuis, Mike Lindmark, Erik Lucero, Dmitry Lyakh, Salvatore Mandrà, Jarrod R. McClean, Matthew McEwen, Anthony Megrant, Xiao Mi, Kristel Michielsen, Masoud Mohseni, Josh

- Mutus, Ofer Naaman, Matthew Neeley, Charles Neill, Murphy Yuezhen Niu, Eric Ostby, Andre Petukhov, John C. Platt, Chris Quintana, Eleanor G. Rieffel, Pedram Roushan, Nicholas C. Rubin, Daniel Sank, Kevin J. Satzinger, Vadim Smelyanskiy, Kevin J. Sung, Matthew D. Trevithick, Amit Vainsencher, Benjamin Villalonga, Theodore White, Z. Jamie Yao, Ping Yeh, Adam Zalcman, Hartmut Neven, and John M. Martinis. Quantum supremacy using a programmable superconducting processor. *Nature*, 574(7779):505–510, October 2019. Publisher: Nature Publishing Group.
- [23] Elizabeth Gibney. Hello quantum world! Google publishes landmark quantum supremacy claim. *Nature*, 574(7779), October 2019.
- [24] C. Neill, P. Roushan, K. Kechedzhi, S. Boixo, S. V. Isakov, V. Smelyanskiy, A. Megrant, B. Chiaro, A. Dunsworth, K. Arya, R. Barends, B. Burkett, Y. Chen, Z. Chen, A. Fowler, B. Foxen, M. Giustina, R. Graff, E. Jeffrey, T. Huang, J. Kelly, P. Klimov, E. Lucero, J. Mutus, M. Neeley, C. Quintana, D. Sank, A. Vainsencher, J. Wenner, T. C. White, H. Neven, and J. M. Martinis. A blueprint for demonstrating quantum supremacy with superconducting qubits. *Science*, 360(6385):195–199, April 2018. Publisher: American Association for the Advancement of Science.
- [25] Nathalie P. de Leon, Kohei M. Itoh, Dohun Kim, Karan K. Mehta, Tracy E. Northup, Hanhee Paik, B. S. Palmer, N. Samarth, Sorawis Sangtawesin, and D. W. Steuerman. Materials challenges and opportunities for quantum computing hardware. *Science*, 372(6539), April 2021. Publisher: American Association for the Advancement of Science.
- [26] Víctor Zapatero, Tim van Leent, Rotem Arnon-Friedman, Wen-Zhao Liu, Qiang Zhang, Harald Weinfurter, and Marcos Curty. Advances in device-independent quantum key distribution. *Quantum Information*, 9(1):1–11, February 2023. Publisher: Nature Publishing Group.

- [27] H.-J. Briegel, W. Dür, J. I. Cirac, and P. Zoller. Quantum Repeaters: The Role of Imperfect Local Operations in Quantum Communication. *Physical Review Letters*, 81(26):5932–5935, December 1998.
- [28] Peter J. Winzer, David T. Neilson, and Andrew R. Chraplyvy. Fiber-optic transmission and networking: the previous 20 and the next 20 years [Invited]. *Optics Express*, 26(18):24190–24239, September 2018. Publisher: Optica Publishing Group.
- [29] A step closer to repeaters for quantum networks. *Nature*, August 2023.
- [30] V. Bužek and M. Hillery. Quantum copying: Beyond the no-cloning theorem. *Physical Review A*, 54(3):1844–1852, September 1996. Publisher: American Physical Society.
- [31] An Illustrated Introduction to Quantum Networks and Quantum Repeaters | AWS Quantum Technologies Blog, November 2022. Section: Quantum Technologies.
- [32] T. Guerreiro, F. Monteiro, N. Bruno, A. Martin, B. Sanguinetti, N. Gisin, N. Sangouard, H. Zbinden, and R. T. Thew. Heralding Photons and Entanglement for Quantum Communication. Optica Publishing Group, March 2014.
- [33] Eric I. Rosenthal, Christopher P. Anderson, Hannah C. Kleidermacher, Abigail J. Stein, Hope Lee, Jakob Grzesik, Giovanni Scuri, Alison E. Rugar, Daniel Riedel, Shahriar Aghaeimeibodi, Geun Ho Ahn, Kasper Van Gasse, and Jelena Vučković. Microwave Spin Control of a Tin-Vacancy Qubit in Diamond. *Physical Review X*, 13(3):031022, August 2023.
- [34] Jean-Michel Borit, Hope Lee, Jakob Grzesik, Daniel Riedel, and Jelena Vučković. Alligator photonic crystal nanoresonators for cavity QED in diamond. In *Bulletin of the American Physical Society*. American Physical Society, 2023.
- [35] Xinghan Guo, Alexander M. Stramma, Zixi Li, William G. Roth, Benchen Huang, Yu Jin, Ryan A. Parker, Jesús Arjona Martínez, Noah Shofer, Cathryn P.

- Michaels, Carola P. Purser, Martin H. Appel, Evgeny M. Alexeev, Tianle Liu, Andrea C. Ferrari, David D. Awschalom, Nazar Deegan, Benjamin Pingault, Giulia Galli, F. Joseph Heremans, Mete Atatüre, and Alexander A. High. Microwave-Based Quantum Control and Coherence Protection of Tin-Vacancy Spin Qubits in a Strain-Tuned Diamond-Membrane Heterostructure. *Physical Review X*, 13(4):041037, November 2023. Publisher: American Physical Society.
- [36] M. Pompili, S. L. N. Hermans, S. Baier, H. K. C. Beukers, P. C. Humphreys, R. N. Schouten, R. F. L. Vermeulen, M. J. Tiggelman, L. dos Santos Martins, B. Dirkse, S. Wehner, and R. Hanson. Realization of a multinode quantum network of remote solid-state qubits. *Science*, 372(6539):259–264, April 2021. Publisher: American Association for the Advancement of Science.
- [37] Perfect imperfections: how AWS is innovating on diamond materials for quantum communication with Element Six | AWS Quantum Technologies Blog, April 2023. Section: Quantum Technologies.
- [38] Carlo Bradac, Weibo Gao, Jacopo Forneris, Matthew E. Trusheim, and Igor Aharonovich. Quantum nanophotonics with group IV defects in diamond. *Nature Communications*, 10(1):5625, December 2019. Publisher: Nature Publishing Group.
- [39] Daniel Riedel, Hope Lee, Jason F. Herrmann, Jakob Grzesik, Vahid Ansari, Jean-Michel Borit, Hubert S. Stokowski, Shahriar Aghaeimeibodi, Haiyu Lu, Patrick J. McQuade, Nicholas A. Melosh, Zhi-Xun Shen, Amir H. Safavi-Naeini, and Jelena Vučković. Efficient Photonic Integration of Diamond Color Centers and Thin-Film Lithium Niobate. *ACS Photonics*, 10(12):4236–4243, December 2023. Publisher: American Chemical Society.
- [40] Yan Qi Huan, Pieter-Jan Stas, David Levonian, Bartholomeus Machielse, Denis Sukachev, Aziza Suleymanzade, Erik Knall, Benjamin Pingault, Can Knaut, Daniel Assumpcao, Yan-Cheng Wei, Mihir Bhaskar, Hongkun Park, Marko Loncar, and Mikhail Lukin. Two-Qubit Nanophotonic Quantum Network Node Using Strained Silicon-Vacancy Spins in Diamond. 2022, January 2022.

- [41] Matthew E. Trusheim, Benjamin Pingault, Noel H. Wan, Mustafa Gündoğan, Lorenzo De Santis, Romain Debroux, Dorian Gangloff, Carola Purser, Kevin C. Chen, Michael Walsh, Joshua J. Rose, Jonas N. Becker, Benjamin Lienhard, Eric Bersin, Ioannis Paradeisanos, Gang Wang, Dominika Lyzwa, Alejandro R-P. Montblanch, Girish Malladi, Hassaram Bakhru, Andrea C. Ferrari, Ian A. Walmsley, Mete Atatüre, and Dirk Englund. Transform-Limited Photons From a Coherent Tin-Vacancy Spin in Diamond. *Physical Review Letters*, 124(2):023602, January 2020. Publisher: American Physical Society.
- [42] Hope Lee, Hannah Kleidermacher, Abigail Stein, Jakob Grzesik, Jean-Michel Borit, Daniil Lukin, Dominic Catanzaro, and Jelena Vuckovic. Cavity Quantum Electrodynamics with Tin Vacancy Centers in Diamond. *Bulletin of the American Physical Society*, 2024. Publisher: APS.
- [43] Daniel Riedel, Immo Söllner, Brendan J. Shields, Sebastian Starosielec, Patrick Appel, Elke Neu, Patrick Maletinsky, and Richard J. Warburton. Deterministic Enhancement of Coherent Photon Generation from a Nitrogen-Vacancy Center in Ultrapure Diamond. *Physical Review X*, 7(3):031040, September 2017. Publisher: American Physical Society.
- [44] Qimin Quan and Marko Loncar. Deterministic design of wavelength scale, ultrahigh Q photonic crystal nanobeam cavities. *Optics Express*, 19(19):18529–18542, September 2011. Publisher: Optical Society of America.
- [45] J. D. Joannopoulos. *Photonic crystals: molding the flow of light*. Princeton University Press, Princeton, 2008.
- [46] J. D. Joannopoulos, Pierre R. Villeneuve, and Shanhui Fan. Photonic crystals. *Solid State Communications*, 102(2):165–173, April 1997.
- [47] Jelena Vuckovic. Quantum Photonics, Spring 2024. Stanford University, CA.
- [48] Purcell, E.W. Proceedings of the American Physical Society. *Physical Review*, 69(11-12):674–674, June 1946. Publisher: American Physical Society.

- [49] Ronan Sauleau. Fabry–Perot Resonators. In *Encyclopedia of RF and Microwave Engineering*. John Wiley & Sons, Ltd, 2005.
- [50] Jonathan Fan. Electromagnetic Waves, Fall 2022. Stanford University, CA.
- [51] Logan Wang Su, Jelena Vuckovic, D. A. B. Miller, and Amir H. Safavi-Naeini. *Computational nanophotonic design: frameworks and applications*. PhD thesis, Stanford University, Stanford, California, 2020.
- [52] Kane Yee. Numerical solution of initial boundary value problems involving maxwell’s equations in isotropic media. *IEEE Transactions on Antennas and Propagation*, 14(3):302–307, May 1966. Conference Name: IEEE Transactions on Antennas and Propagation.
- [53] Logan Su, Dries Vercauteren, Jinhie Skarda, Neil V. Sapiro, Jan A. Petykiewicz, and Jelena Vučković. Nanophotonic inverse design with SPINS: Software architecture and practical considerations. *Applied Physics Reviews*, 7(1):011407, March 2020.
- [54] Martin F. Schubert, Alfred K. C. Cheung, Ian A. D. Williamson, Aleksandra Spyra, and David H. Alexander. Inverse Design of Photonic Devices with Strict Foundry Fabrication Constraints. *ACS Photonics*, 9(7):2327–2336, July 2022. Publisher: American Chemical Society.
- [55] Geun Ho Ahn, Ki Youl Yang, Rahul Trivedi, Alexander D. White, Logan Su, Jinhie Skarda, and Jelena Vučković. Photonic Inverse Design of On-Chip Microresonators. *ACS Photonics*, 9(6):1875–1881, June 2022. Publisher: American Chemical Society.
- [56] Jesse Lu, Stephen Boyd, and Jelena Vučković. Inverse design of a three-dimensional nanophotonic resonator. *Optics Express*, 19(11):10563–10570, May 2011. Publisher: Optica Publishing Group.
- [57] Jean-Michel Borit, Jakob Grzesik, Hannah Kleidermacher, Hope Lee, Abigail Stein, and Jelena Vuckovic. Inverse-designed nanophotonic resonators for cavity

- QED in diamond. *Bulletin of the American Physical Society*, 2024. Publisher: APS.
- [58] Xinghan Guo, Mouzhe Xie, Anchita Addhya, Avery Linder, Uri Zvi, Tanvi D. Deshmukh, Yuzi Liu, Ian N. Hammock, Zixi Li, Clayton T. DeVault, Amy Butcher, Aaron P. Esser-Kahn, David D. Awschalom, Nazar Deegan, Peter C. Maurer, F. Joseph Heremans, and Alexander A. High. Direct-bonded diamond membranes for heterogeneous quantum and electronic technologies, June 2023.
- [59] Ziwei Zhu and Changxi Zheng. Differentiable scattering matrix for optimization of photonic structures.
- [60] Mark Brongersma and Shanhui Fan. Nanophotonics, Fall 2023. Stanford University, CA.
- [61] David J Griffiths. Introduction to Electrodynamics. 2013.
- [62] Norman Hodgson and Horst Weber. The Fabry Perot Resonator. In Norman Hodgson and Horst Weber, editors, *Optical Resonators: Fundamentals, Advanced Concepts and Applications*, pages 137–162. Springer, London, 1997.